 SDHM, vol.6, no.4, pp.273-288, 2010

Fracture Behavior in AFM-Specimen with Single Crack under Different Loading Conditions

Qing-fen Li[1], Li Zhu[1], Shi-fan Zhu[1] and F-G Buchholz[1]

Abstract: The fracture behavior in all fracture mode (AFM)-specimen with a single edged crack under different loading conditions is investigated by the aid of the commercial ANSYS code. The separated strain energy release rates (SERRs) along the crack front are calculated by the modified virtual crack closure integral (MVCCI)-method. It is shown that the computational results of the AFM-specimen are in good agreement with some available findings for pure mode I, mode II, mode III, and mixed-mode I+III loading conditions. Furthermore, the crack growth problems under complex mixed-mode II+III loading condition by using the AFM-specimen, are investigated and results show that once mode II and mode III loads are superimposed, the distributions of the SERRs values are no longer symmetric with respect to the middle point of the crack front. The maximum total SERRs value occurs at z/t=0.5. It can therefore be predicted that under mixed-mode II+III loading condition, fracture will initiate at one corner along the crack front of the AFM-specimen.

Keywords: Fracture behavior, all fracture mode (AFM)-specimen, strain energy release rates (SERRs), modified virtual crack closure integral (MVCCI)-method, mixed-mode loading conditions.

1 Introduction

Fracture processes are in many cases of the three dimensional (3D) character in the real engineering structures, where cracks may experience superimposed tensile, shear and torsional stress for the complex geometries and loading conditions. However, only a few 3D fracture criteria have been proposed so far [Citarella and Cricrì (2010); Pook (1995); Dhondt (2003); Sih and Cha (1974); Chang, Xu, and Mutoh (2006)], and the prediction of the developing 3D fracture process is not well understood yet. Previously, two-dimensional crack extension problems under mixed-mode I and II loading conditions have attracted much attention and through many

[1] College of Mechanical and Electrical Engineering, Harbin Engineering University, Harbin, China

investigations the problem is now well understood. There is a standardized test procedure for determining the fracture toughness value K_{Ic} and this value is already known for many materials [Richard and Kuna (1990)]. Besides, a number of fracture criteria for predicting the initiation and the direction of fatigue crack growth under mixed-mode I and II crack tip loading conditions are well established [Buchholz and Richard (2000)]. For the corresponding 3D case, however, theoretical and experimental studies have only just begun to deal with a combination of all three fracture modes since last decade [Buchholz and Richard (2004)]. No standardized test procedures or specimens can determine the K_{IIc} and K_{IIIc} values [Richard and Kuna (1990)]; only very limited experimental works are available [Pook (1995); Hull (1994); Richard and Kuna (1990); Davenport and Smith (1993)]. In particular there is a shortage of experimental findings regarding general 3D and mixed-mode fracture to form a solid basis on which the desired understanding and the missing fracture criteria could be established [Richard and Kuna (1990)].

The finite element method (FEM) has been used with great success in the computational fracture mechanics in the past several decades, and the boundary element method (BEM) is well established as an effective alternative to the FEM. In recent years, several promising methods of modelling have been developed. The dual boundary element method (DBEM) has been used for complex structural models [Aliabadi (1997); Cisilino and Aliabadi (1999); Dirgantara and Aliabadi (2001); Aliabadi and Saleh (2001); Wang and Yao (2006)]. The extended finite element method (XFEM) originally proposed by Belytschko in 1999 [Moes, Dolbow, and Belytschko (1999)] is very powerful for discontinuous problems in mechanics [Belytschko, Lu, and Gu (1994); Jun, Liu, and Belytschko (1998); Belytschko, Krongauz, Organ, Fleming, and Krysl (1996)]. And it is effective to take advantage of the Meshless method to analyse the Fracture Mechanics problems such as crack propagation [Wen and Aliabadi (2010); Chen, Eskandarian, Oskard, and Lee (2004); Belytschko, Guo, Liu, and Xiao (2000)]. Although the investigation of 3D crack configurations has been a major task of fracture-mechanical research for a long time, the description of the crack deflection under general mixed-mode loading is still unsolved. Further investigations have to be performed in order to improve this situation.

In this paper, the AFM-specimen with its special loading device proposed by Richard [Richard and Kuna (1990)] is presented and the fracture behavior for different loadings is discussed by finite element (FE) analysis. The computational fracture analysis is based on the calculation of separated strain energy release rates (SERRs) along the crack front by the modified virtual crack closure integral (MVCCI)-method [Rybicki and Kanninen (1977)] and the commercially available FE-code ANSYS.

2 FE-model of the AFM-specimen and loading conditions

The AFM-specimen mounted in the loading device is displayed in Fig. 1 a) and the AFM-specimen is shown in Fig. 1 b). The loading device consists of two specially designed parts of spheres, as illustrated in Fig. 1 a), through which the load F of a standard uniaxial tensile/compression testing machine is introduced. The middle part of AFM-specimen (Fig. 1 b)) can be considered as a special type of single edge notched (SEN) specimen with a straight crack perpendicular to the free surface. The design is such that the load line intersects the center of the AFM-specimen and the notch that is machined there. The cross-section of the specimen with the reference coordinate system is illustrated in Fig. 1 c). The coordinate origin is positioned at the middle point of the crack front of the specimen. For further details reference is given by Richard [Richard and Kuna (1990)].

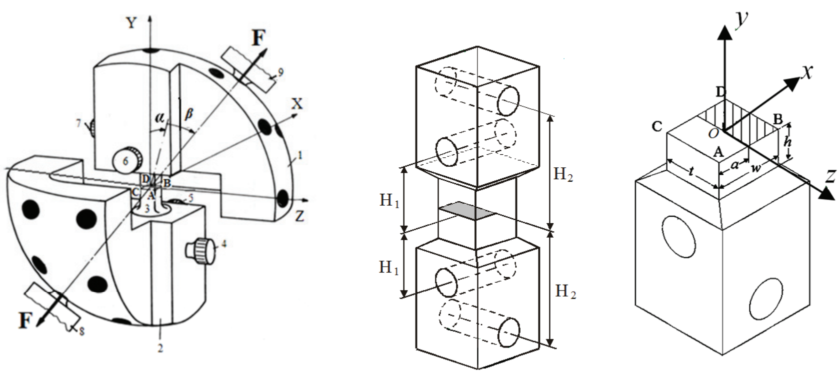

a) b) c)

Figure 1: a) Loading device of AFM-specimen b) AFM-specimen c) Crack plane cross section

Through the loading device, the AFM-specimen is loaded by force F from angles α and β; the normal force N, the shearing forces Q and T and the bending moments M_Q and M_T are induced in three basic loading conditions, see Fig. 2.

M_Q and M_T are to compensate for the moments of the shearing forces Q and T with respect to the coordinate origin, so that only the normal force N and the shearing forces Q and T are acting upon the cross-section ABCD of the specimen. The values of each of these can be expressed in relation to the angle of force introduction as follows:

$$F_y = N = F\cos\alpha\cos\beta \tag{1}$$

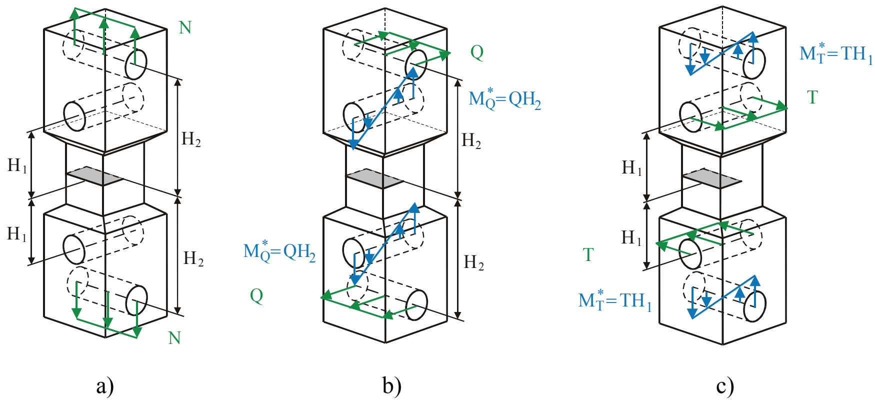

Figure 2: Three basic loading conditions: a) Tension b) In-plane shear c) Out-of-plane shear

$$F_x = Q = F \sin\alpha \cos\beta \tag{2}$$

$$F_z = T = F \sin\beta \tag{3}$$

$$M_Q = F H_2 \sin\alpha \cos\beta \tag{4}$$

$$M_T = F H_1 \sin\beta \tag{5}$$

In the conducting of fracture mechanics analyses, the AFM-specimen dimensions, in Fig. 1 b) and c), are as follows: width w=27mm, height h=20mm, thickness t =0.9 w, normalized crack length a =0.5 w(straight crack front), H_1 =32.5mm, and H_2 =57.5mm. The material parameters are chosen as follows: Young's modulus E=2.1 $\times$ 10^5N/mm^2 and Poisson's ratio ν =0.3. The specimen is subject to a static loading of F=6561N.

The whole part, the center part, and the crack plane cross section of 3D FE-model of the AFM-specimen are shown in Fig. 3 a)-c) respectively. The whole model (Fig. 3 a)) is assembled of some standard 6- but predominantly of non-singular, standard 8-node volume elements, also along the crack front, and has about 30, 000 degrees of freedoms. Considering the singular stress behavior at the crack front moderate mesh refinement (Fig. 3 c)) is incorporated in the model adjacent to the crack front, and with respect to the MVCCI-method the crack front is formed by a homogeneous mesh with elements of constant size ($0.1 \times 0.1 \times 0.1$mm with$\Delta a =$ 0.1mm and $\Delta a/a = 0.0074$).

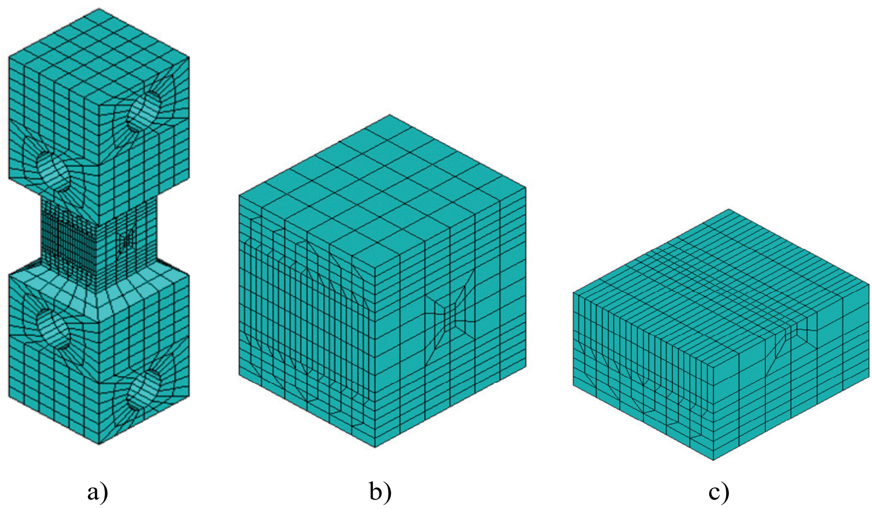

Figure 3: 3D FE-model of the AFM-specimen: a) Whole part b) Center part c) Crack plane cross section

3 Validation of FE-model for 3D computational analyses

In order to verify the accuracy of the MVCCI-method, regarding the FE-mesh and the chosen elements, the case should be considered primitively that the center part of the AFM-specimen under pure tension loading condition (α = 0° and β = 0°). Considering that the specimen ends serve as transmitting force, the center part of the AFM-specimen can simulate SEN-specimen, particularly in combination with suppressed displacements in the thickness- or z-direction of the specimen (see Fig. 4 a)). By this trick, plane strain boundary conditions (BCs) are enforced on the 3D-model of the center part. With the pressure $\sigma_{yy} = -10N/mm^2$ applied to upper and lower cross sections (see Fig. 4 b)-c)), the SERRs evaluated along the crack front are constant. Compared to the corresponding 2D reference value [Murakami (1978)], the small relative error of Δ_{rel}=2.336%, reveals that this 3D FE-model of the AFM-specimen and the MVCCI-method can be assessed as qualified for the analyses of general 3D cases.

4 Comparisons between the AFM-results and the 3PB- or 4PS-findings

For advanced 3D crack growth under general and variable mixed mode loading conditions along the crack front, the pronounced experimental findings presented and discussed so far, are the cases of the three point bending (3PB) specimen with

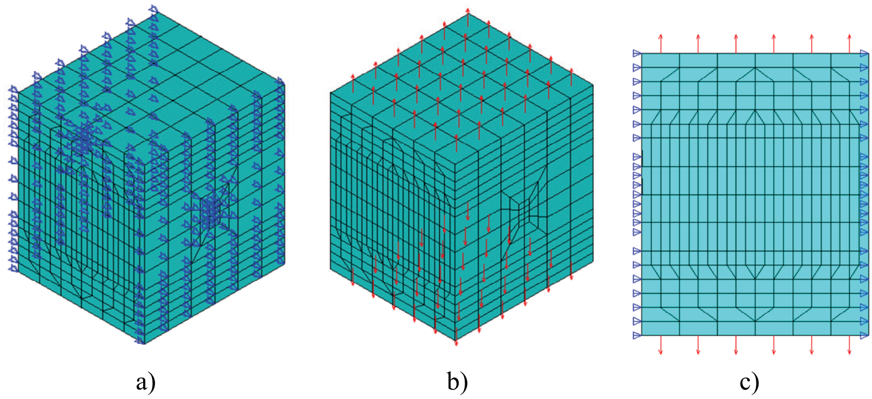

Figure 4: Center part of the AFM-specimen under pure tension loading condition: a) Plain strain BCs in axonometric view b) Pressure in axonometric view c) Loads and BCs in front view

a crack perpendicular or inclined to the mid plane between the supports, and four point shear (4PS) specimen with a straight crack under in-plane or out-of-plane shear loading conditions, at the Institute of Applied Mechanics of the University of Paderborn [Buchholz, Chergui, and Richard (2004)]. The computational and experimental findings of the 3PB- and 4PS-specimens can benefit for examining and interpreting the computational results of the AFM-specimen, with respect to the pure mode I, pure mode II, pure mode III, and mixed-mode I+III loading conditions in this paper, even though the geometry dimension of the AFM-specimen are different from the 3PB- and the 4PS-specimens.

Due to the symmetry of the problem only half of the specimens ($z/t \geq 0$) are considered for pure mode I, pure mode II, pure mode III, and mixed-mode I+III loading conditions, since the AFM- and 3PB/4PS-results in these cases are symmetric with respect to the middle point along the crack front.

4.1 AFM- and 3PB-specimens under mode I loading condition

The analyzed results of AFM-specimen under pure tension loading condition ($\alpha = 0^\circ$ and $\beta = 0^\circ$) are illustrated in Fig. 5 a), and compared with the results of 3PB-specimen with a straight crack under pure tension loading condition from reference [Buchholz, Chergui, and Richard (2004)] in Fig. 5 b).

Fig. 5 a) shows that rather constant values of G_{In} are generated along the crack front in the inner part of the AFM-specimen ($|z/t| \leq 0.3$) and slightly decreasing values of G_{In} are detected where the crack front meets the free surfaces of the specimen

($|z/t| \rightarrow 0.5$). From Fig. 5 b), the G_{In} values are found to be nearly constant in the inner part of the 3PB-specimen ($|z/t| \leq 0.25$) and the decreasing values of G_{In} at $|z/t| \rightarrow 0.5$ can also be noticed.

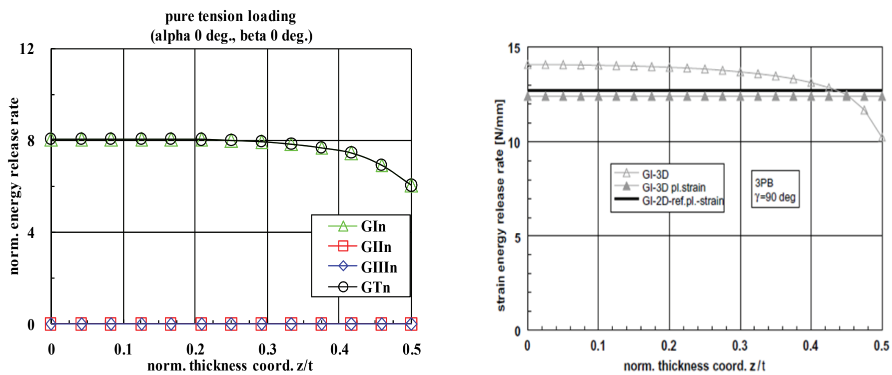

a) b)

Figure 5: Normal SEERs under mode I loading condition for: a) AFM-specimen b) 3PB-specimen [Buchholz, Chergui, and Richard (2004)]

The decrease of SERRs values is well known as 3D-effect, which is related to Poisson's ratio and the laterally less constrained strains along the crack front adjacent to the free surfaces of the specimen. Where, the surface displacement can be clearly recognized in the corresponding mesh details in Fig. 6 a)-c). Certainly the slightly curved and convex crack fronts, which are found in most fatigue experiments of mode I, are correlated to this 3D effect through reduced fatigue crack growth rates for$|z/t| \rightarrow 0.5$ [Buchholz, Chergui, and Richard (1999)].

4.2 AFM- and 4PS-specimens under mode II loading condition

The calculated results of the AFM-specimen under in-plane shear loading condition ($\alpha = 90^{\circ}$and $\beta = 0^{\circ}$) are given in Fig. 7 a) and the 4PS-specimen results by [Buchholz, Chergui, and Richard (2004)] are given in Fig. 7 b). Results show that the generated G_{IIn}-curve of the AFM-specimen is similar to the one of 4PS-specimen, where both the G_{IIn}-values are rather constant in the inner part of the specimen, and show remarkably increasing for $|z/t| \rightarrow 0.5$. Meanwhile, the G_{IIIn}-values occur locally along the crack front of both AFM- and 4PS-specimens, even though there is no out-of-plane shear loading component applied. This behavior is due to a weak mode coupling effect between mode II and mode III, which is related to

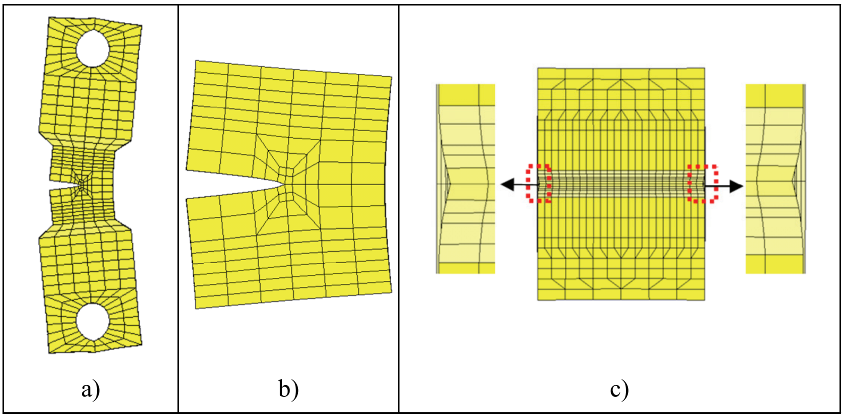

Figure 6: Deformed FE-model of the AFM-specimen under mode I loading condition (Displacement Magnification Factor (DMF)=350) a) Full part in right view b) Center part in right view c) Center part in front view and crack corners in enlarged view

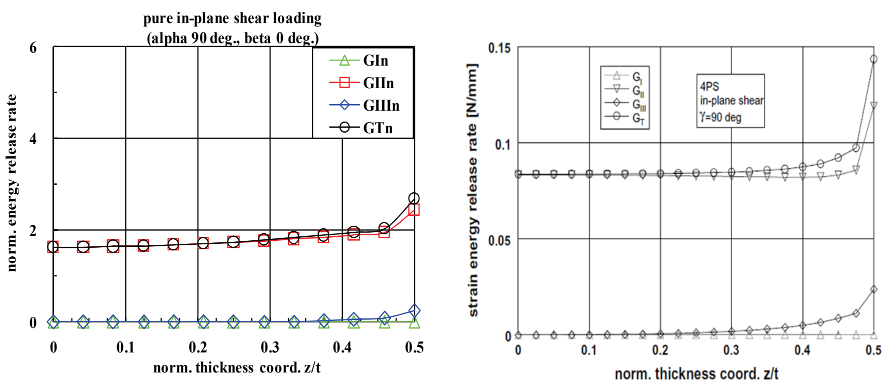

a) b)

Figure 7: Normal SEERs under mode II loading condition for: a) AFM-specimen b) 4PS-specimen [Buchholz, Chergui, and Richard (2004)]

Poisson's ratio and the laterally less constrained strains adjacent to the free surface of the specimen as stated in ref [Buchholz, Chergui, and Richard (2004)].

The weak mode coupling effect can be illustrated qualitatively in different views of the deformed FE-model in Fig. 8. The in-plane sliding displacements of the crack faces can be obviously noticed in Fig. 8 a) and b). Nevertheless, in the front view and especially in the enlarged view of the same crack tip (Fig. 8 c)), some out-of-plane sliding displacements of the crack faces can be recognized at the corners where the crack front meets the free front surfaces of the specimen.

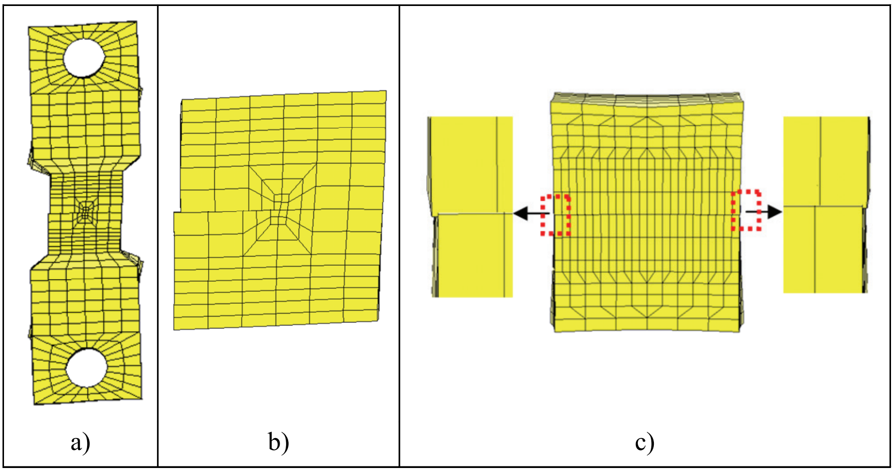

Figure 8: Deformed FE-model of the AFM-specimen under mode II loading condition (Displacement Magnification Factor (DMF)=350): a) Full part in side view b) Center part in side view c) Center part in front view and crack corners in enlarged view

4.3 AFM- and 4PS-specimens under mode III loading condition

The AFM-results under out-of-plane shear loading condition (α =0°, β =90°) are shown in Fig. 9 a), and the 4PS-results [Buchholz, Chergui, and Richard (2004)] in Fig. 9 b). Results show that the G_{IIIn}-values of AFM decrease slowly along the crack front for $|z/t| \leq 0.3$ and increase slightly only for $|z/t| \rightarrow 0.5$, which is in agreement with the previous findings of the 4PS-results. In addition, for $|z/t| \geq 0.25$ especially for $|z/t| \rightarrow 0.5$, remarkably increasing G_{IIn} values occur for both AFM- and 4PS-specimens, since the G_{IIn}-values are locally induced along the crack front by the strong mode coupling effect between mode III and mode II, which is related to the global deformation behavior of specimen as experimentally confirmed in ref [Buchholz, Chergui, and Richard (2004)].

The corresponding deformed FE-model of the AFM-specimen under mode III is shown in Fig. 10. It is obvious that besides the globally torsion behavior (Fig. 10 a) and b)), the in-plane displacements (Fig. 10 c) and d)) are induced by the locally induced mode II loading condition.

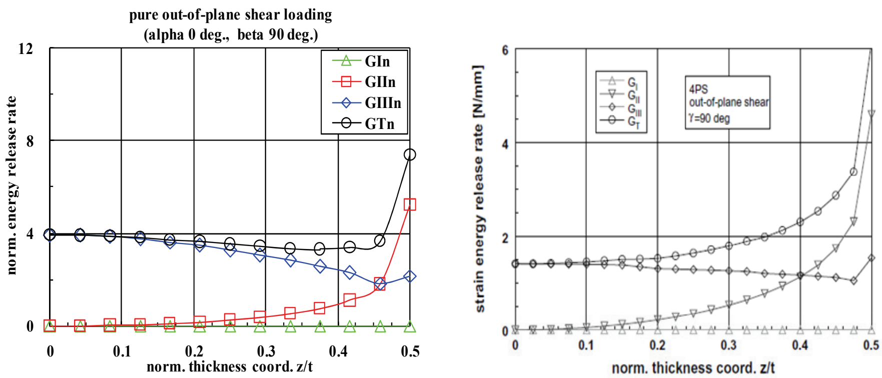

a) b)

Figure 9: Normal SEERs under mode III loading condition for: a) AFM-specimen b) 4PS-specimen [Buchholz, Chergui, and Richard (2004)]

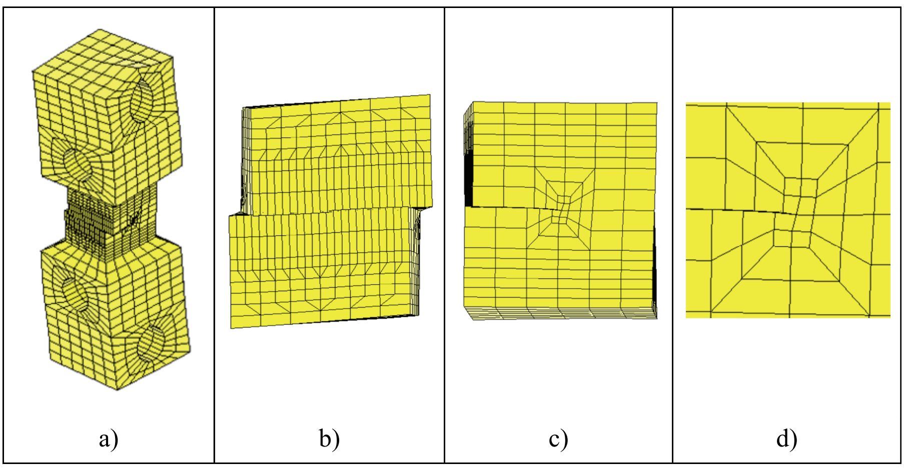

Figure 10: Deformed FE-model of the AFM-specimen under mode III loading condition (Displacement Magnification Factor (DMF)=350): a) Full part in axonometric view b) Center part in front view c) Center part in side view d) Crack tip in enlarged view

4.4 AFM- and 3PB-specimens under mode I+III loading condition

The AFM-results under mixed-mode I+III loading condition ($\alpha = 0^{\circ}$and $\beta = 45^{\circ}$) are illustrated in Fig. 11 a), and the 3PB-results [Buchholz, Chergui, and Richard

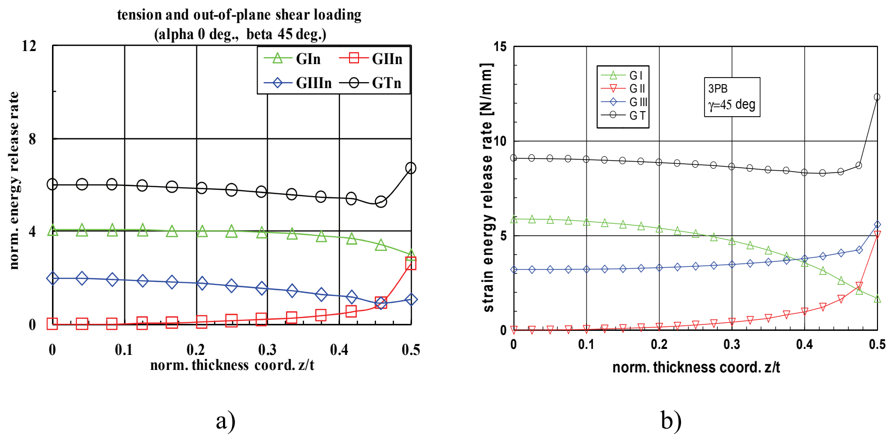

Figure 11: Normal SEERs for mixed-mode I+III loading condition for: a) AFM-specimen b) 3PB-specimen [Buchholz, Chergui, and Richard (2004)]

(2004)] are in Fig. 11 b). In this case, mode I and mode III loading conditions are generated along the straight crack front by applying spatial loading on AFM-specimen. The G_{In}-values of the AFM-specimen decrease slightly when $|z/t| \geq 0.25$ and remarkably when $|z/t| \rightarrow 0.5$, which are similar to the 3PB results. This behavior is also related to the 3D-effect as aforementioned in section 4.1. Inevitably, in this case, mode II loading conditions are induced locally along the crack front of the AFM-specimen. Here, G_{IIn}-values of AFM are induced for$|z/t| \geq 0.25$, and increase significantly for $|z/t| \rightarrow 0.5$, which is similar to 3PB-specimen.

The related FE-model and especially the deformed crack tip details are given in Fig. 12 a) –d). From which, the expected crack opening- and out-of-plane sliding displacements can be observed (Fig. 12 a) and b)), and the in-plane sliding displacements of the crack faces can be clearly recognized in Fig. 12 c) and d).

5 Analyses of the AFM-specimen under mixed-mode II+III loading condition

Investigations for pure mode I, mode II, mode III, and mixed-mode I+III loading conditions have been successfully presented by 3PB- and 4PS-specimens in ref [Buchholz, Chergui, and Richard (2004)]. The present work by AFM-specimen is in good agreement with them as mentioned above. However, the fracture behavior under mode II+III loading condition are not available yet. By using the AFM-specimen, the crack growth problems under complex mixed-mode II+III loading condition is actable investigated in this section.

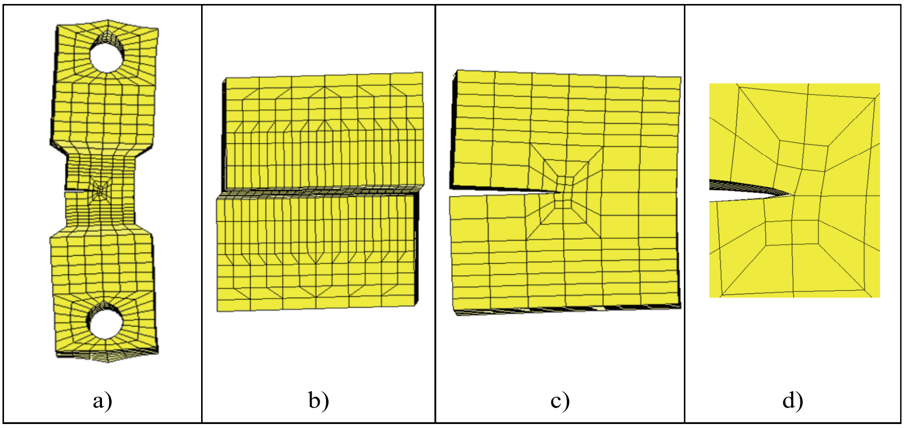

Figure 12: Deformed FE-model of the AFM-specimen under mixed-mode I+III loading condition (Displacement Magnification Factor (DMF)=350): a) Full part in front view b) Center part in front view c) Center part in side view d) Crack tip in enlarged view

The SEERs results along the crack front of the AFM-specimen under mixed-mode II+III loading condition (α =90°, β =45°) are given in Fig. 13. It is apparent that the distributions of the SERRs values are no longer symmetric with respect to the middle point of the crack front. The G_{IIn}-values for*z*/*t*<0 are obviously smaller than those for *z*/*t* $\geq$0. This behavior is owing to that the external out-of-plane shear loading component induces a global torsional deformation which leads the in-plane shear loading condition locally along the crack front of the AFM-specimen, as aforementioned in section 4.3. Accordingly, for *z*/*t* <0, the induced in-plane shear loads and the external applied in-plane shear loads along the crack front are in opposite direction, whereas for *z*/*t* $\geq$0, the two mode loads are both in the positive direction. Consequently, the G_{IIn} (*z*/*t* <0)-values are the results of that the applied mode loads offset the induced ones, whereas the G_{IIn}(*z*/*t* $\geq$0)-values are the results of that the applied mode loads plus the induced ones. Besides, owing to the weak mode coupling effect as aforesaid in section 4.2, the external in-plane shear loading component also induces an out-of-plane shear loading component which is negative for *z*/*t*<0 and positive for*z*/*t* $\geq$0.

Finally, the maximum total SERRs value, G_{Tn}, occurs at *z*/*t*=0.5 (see Fig. 13). It can therefore be predicted that under mixed-mode II+III loading condition, the fracture will occur initially at one corner on the crack front of the AFM-specimen.

Qualitatively, the deformed crack details of the FE-model of the AFM-specimen

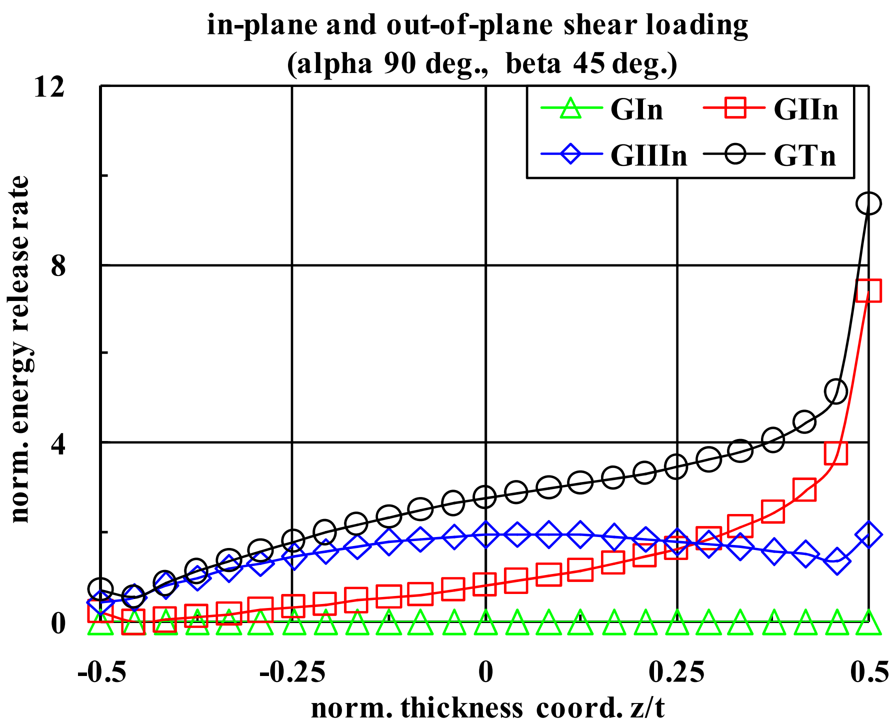

Figure 13: Normal SEERs along the crack front of the AFM-specimen for mixed-mode II+III loading condition

under mixed-mode II+III loading condition are given in Fig. 14. For side views, we can see that the in-plane slide displacements for $z/t \rightarrow -0.5$ (left view, Fig. 14 a)) are not as obvious as the ones for $z/t \rightarrow +0.5$ (right view, Fig. 14 c)). From top view (Fig. 14 b)), we can see that the out-of-plane slide displacements for$z/t \rightarrow +0.5$are more obvious than the ones for $z/t \rightarrow -0.5$.

6 Conclusions

The detailed results of computational 3D crack fracture behavior have been presented by using AFM-specimen. By applying plane strain boundary conditions (BCs) to the 3D FE-model of the center part of the AFM-specimen, the SERRs results can be compared with 2D reference value. The minimal relative error shows that the 3D FE-model of AFM-specimen and the MVCCI-method are validated for general 3D analyses.

The computational results of the AFM-specimen are in good agreement with the

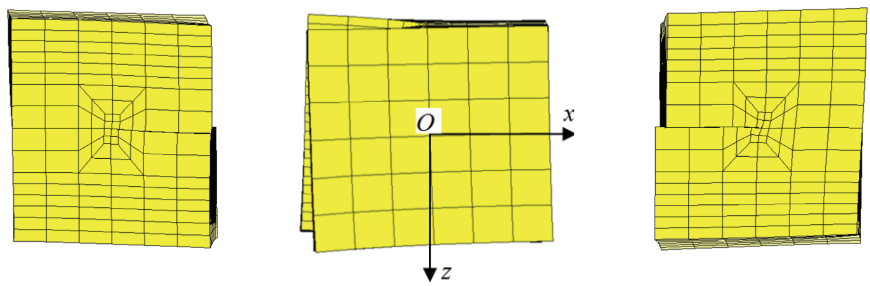

a) b) c)

Figure 14: Deformed crack details of the AFM-specimen under mixed-mode II+III loading condition (Displacement Magnification Factor (DMF)=350): a) Left view b) Top view c) Right view

available findings of the 3PB- and 4PS-specimen for mode I, mode II, mode III, and mixed-mode I+III loading conditions. It reveals that the computational analyses by AFM-specimen are reasonable.

Furthermore, by using the AFM-specimen, the complex fracture behavior under mixed-mode II+III loading condition is investigated. The computational results show that once the mode II and III loads are applied together on the specimen, the distributions of the SERRs values are no longer symmetric with respect to the middle point of the crack front. The G_{IIn}- and G_{IIIn}-values are influenced by both the weak mode coupling and the global torsional deformation effects. The maximum total SERRs value occurs at z/t=0.5. It can therefore be predicted that under mixed-mode II+III loading condition, fracture will initiate at one corner along the crack front of the AFM-specimen.

Acknowledgement: This paper is devoted to the memory of Professor Fritz Buchholz. The authors Li Qing-fen, Zhu Li and Zhu Shi-fan gratefully acknowledge Professor Fritz Buchholz for his guidance and helpful discussion in the present work. They will never forget the many years of collaboration and friendship with him. Professor Fritz Buchholz will be always in the memories of all his colleagues, friends and students in College of Mechanical and Electrical Engineering, Harbin Engineering University.

References

Aliabadi, M.H. (1997): A new generation of boundary element methods in fracture mechanics. *International Journal of Fracture*, vol. 86 (1-2), pp. 91-125.

Belytschko, T.; Guo, Y.; Liu, W.K.; Xiao, S.P. (2000): A unified stability analysis of meshless particle methods. *International Journal for Numerical Methods in Engineering*, 48 (9), pp. 1359-1400.

Belytschko, T.; Krongauz, Y.; Organ, D.; Fleming, M.; Krysl, P. (1996): Meshless methods: An overview and recent developments. *Computer Methods in Applied Mechanics and Engineering*, vol. 139 (1-4), pp. 3-47.

Belytschko, T.; Lu, Y.Y.; Gu, L. (1994): Element-free Galerkin methods. *International Journal for Numerical Methods in Engineering*, vol. 37 (2), pp. 229-256.

Aliabadi, M.H.; Saleh, A.L. (2001): Fracture mechanics analysis of cracking in plain and reinforced concrete using the boundary element method. *Engineering Fracture Mechanics*, vol. 69 (2), pp. 267-280.

Buchholz, F.-G; Chergui, A.; Richard, H.A. (2004): Fracture analyses and experimental results of crack growth under general mixed mode loading conditions. *Engineering Fracture Mechanics*, vol. 71, pp. 455-468.

Buchholz, F.-G; Chergui, A.; Richard, H.A. (1999): Computational fracture analyses by means of virtual crack closure integral methods. In: C. Garcia Garino *et al.CD-ROM-Proceedings of the 6th Congreso Argentino de Mecanica Computational (MECOM99), Mendoza, Argentina, September 1999*, Asociación Argentina de Mecánica Computacional, Santa Fe, pp. 316.

Buchholz, F.-G.; Richard, H.A. (2000): Optimisation of the AFM-specimen with respect to advanced fracture and fatigue investigations: *Proc. of the Int. Symposium, Meso-Mechanical Aspects of Material Behavior*, pp. 1-17.

Buchholz, F.-G.; Richard, H.A. (2004): Comparison of computational crack path predictions with experimental findings for SEN-specimens under different loadings: *WCCM VI in conjunction with APCOM'04*, pp.129-132

Chang, J.; Xu J.-Q.; Mutoh, Y. (2006): A general mixed-mode brittle fracture criterion for cracked materials, *Engineering Fracture Mechanics*, vol. 73 (9), pp. 1249-1263.

Chen, Y.; Eskandarian, A.; Oskard, M.; Lee, J.D. (2004): Meshless analysis of plasticity with application to crack growth problems. *Theoretical and Applied Fracture Mechanics*, vol. 41 (1-3), pp. 83-94.

Cisilino, A.P.; Aliabadi M.H. (1999): Three-dimensional boundary element analysis of fatigue crack growth in linear and non-linear fracture problems. *Engineering Fracture Mechanics*, vol. 63 (6), pp. 713-733.

Citarella, R.; Cricrì, G. (2010): Comparison of DBEM and FEM crack path predictions in a notched shaft under torsion. *Engng. Fract. Mech.*, pp. 1730-1749.

Davenport, J. C. W.; Smith D. J. (1993): A study of superimposed fracture modes I, II and III on PMMA. Engng. *Mater. Struct.*, vol. 16, pp. 1125-1133.

Dhondt, G. (2003): A new three-dimensional fracture criterion. *Key Engineering Materials*, vol. 251-252, pp. 209-214.

Dirgantara, T.; Aliabadi, M.H. (2001): Dual boundary element formulation for fracture mechanics analysis of shear deformable shells. *International Journal of Solids and Structures*, vol. 38 (44-45), pp. 7769-7800.

Hull, D. (1994): The effect of mixed mode I/III on crack evolution in the brittle solids. *Int. J. Fract.*, vol. 70, pp. 59-79.

Jun, S.; Liu, W.K.; Belytschko, T. (1998): Explicit reproducing kernel particle methods for large deformation problems. *International Journal for Numerical Methods in Engineering*, vol. 41 (1), pp. 137-166.

Moës, N.; Dolbow, J.; Belytschko T. (1999): A finite element method for crack growth without remeshing. *International Journal for Numerical Methods in Engineering*, vol. 46(1), pp. 131-150.

Murakami, Y. (1978): *Stress Intensity Factors Handbook.* Pergamon Press, Oxford, Vol. 1, pp. 94-96.

Pook, L.P. (1995): On fatigue crack paths. *International Journal of Fatigue*, vol. 17 (1), pp. 5-13.

Richard, H. A.; Kuna. M. (1990): Theoretical and experimental study of superimposed fracture modes I, II and III. *Engineering fracture Mechanics*, vol. 35, no. 6, pp. 949-960.

Rybicki, E. F.; Kanninen, M. F. (1977): A finite element calculation of stress intensity factors by a modified crack closure integral. *Engng. Fract. Mech.*,vol. 9, pp. 931-938.

Sih, G.C.; Cha, B.C.K. (1974): A fracture criterion for three-dimensional crack problems. *Engineering Fracture Mechanics*, vol. 6 (4), pp. 699-723.

Wang, P.B.; Yao, Z.H. (2006): Fast multipole DBEM analysis of fatigue crack growth. *Computational Mechanics*, vol. 38 (3), pp. 223-233.

Wen, P.H.; Aliabadi, M.H. (2010): Mixed-mode stress intensity factors by mesh free galerkin method. *Key Engineering Materials*, vol. 417-418, pp. 957-960.